J Mater Sci: Mater Electron (2023) 34:440

Astragalus brachycalyx fischer roots-derived porous carbon integrated with a novel $NiSnO_2$/PC nanocomposite for high-performance supercapacitors

Serkan Demirel[1], Mehmet Salih Nas[2], Adem Kocyigit[3,*], Mehmet Harbi Calimli[4], and Mehmet Hakkı Alma[2]

[1] Department of Electricity and Energy, Igdir University, 76000 Igdir, Turkey
[2] Department of Environmental Engineering, Faculty of Engineering, Iğdır University, 76000 Iğdır, Turkey
[3] Department of Electronics and Automation, Vocational High School, Bilecik Şeyh Edebali University, 11230 Bilecik, Turkey
[4] Department of Medical Services and Techniques, Tuzluca Vocational School, Iğdır University, 76000 Iğdır, Turkey

Received: 26 August 2022
Accepted: 15 January 2023
Published online: 4 February 2023

ABSTRACT

The $NiSnO_2$/biomass-derived porous carbon (PC) composites were synthesized from the roots of *Astragalus brachycalyx* fischer by using a series of physico-chemical processes. Then, the composites were characterized by XRD, SEM, BET, Raman and EDS to illuminate and confirm the structures. The $NiSnO_2$/biomass-derived PCs were employed as a new class of renewable supercapacitor electrodes. The electrochemical performance of the prepared PC electrodes was analyzed by using two electrodes in a 6 M potassium hydroxide (KOH) aqueous solution electrolyte. Electrochemical measurements revealed that $NiSnO_2$/PC nanocomposites demonstrated highly effective stability with a specific capacitance of 295.90 F/g at 200 mV/s for supercapacitor studies, and a capacitance retention rate of 38.70% after 200 cycles. The high surface area and the presence of large hierarchical pores contributed to the effective electrochemical performance of the prepared nanocomposite materials. The $NiSnO_2$/PC nanocomposites with the 3D porous structure have showed that promising efficiency in the application of supercapacitors with its high energy storage capacity and effective electrochemical performance.

1 Introduction

The energy demands of the world mostly depend on fossil fuels that are the main reason for global warming in the twenty-first century. Thus, increasing concerns related to fossil fuels and the environmental pollution have triggered many research efforts for alternative energy sources and related electronic devices [1, 2]. The development of electronic devices and their role in our lives have increased the importance of these devices [3, 4]. Recently, electrical-

Address correspondence to E-mail: adem.kocyigit@bilecik.edu.tr

https://doi.org/10.1007/s10854-023-09894-7

based energy storage devices like batteries and supercapacitors have taken great attention due to their environment-friendly energy production and portability [5–8]. The supercapacitors exhibit superior features such as low cost, high power density, safe operation process, fast charge–discharge rate, long cycle life and less maintenance compared to batteries [9–11]. Because of these advantages, supercapacitors have been evaluated seen excellent candidates of energy storage source to be replaced with batteries [12–15]. The charge storage mechanism of supercapacitors operates depends on in two ways. The first one of them is electron transfer in an electrolytic solution, and another is electrolytic double-layer formation on the electrode surface or inside the electrolyte [2, 16]. Supercapacitors are effective in supplying high power needs suddenly and can be charged externally with batteries in normal operation. However, they are still insufficient in energy intensity compared to batteries [17]. Energy intensity can be improved by regulating device capacitance and potential [18]. There are many efforts to improve supercapacitors. For example, Li et al. synthesized porous carbon from some of plants and obtained high specific capacitance of 568 F/g [19]. Wang et al. obtained carbon microspheres from hemicelluloses and reached high specific capacitance value of 218 F/g after activaton of spheres [20].

The materials used in the electrodes need to be extremely effective for improving the electrochemical performance of supercapacitors [21, 22]. For that reason, various supporting materials such as multi-walled carbon nanotube [2, 3], activated carbon [23], polymers [24], graphenes [25], carbon fibers [26], etc., have been used in the production of supercapacitors electrodes. Nowadays, porous carbon (PC) derived from various sources like fruit peels [27], raw cotton [28] and baobab fruit peel [29] have been popularly used as electrode materials [30–32]. High stability, good conductivity, large surface area and low cost have led to the intensive use of PC materials as an electrode [28, 33]. Synthesis of cost-effective and sustainable electrodes with good porosity, heteroatom structure and diverse functional groups are very important for desired supercapacitors [29]. According to the abovementioned advantages, carbon-based materials can store and adsorb a large number and variety of ions due to their large spherical surface area and porous structure. Thus, the carbon-based materials can show double-layer capacitance with high electrical conductivity performance [34]. To improve electrochemical performance of PC, several metals have been loaded to carbon-based materials for supercapacitors applications. For instance, transition metal oxide of Ru, Co and Mn has been used in the fabrication of electrode materials of pseudocapacitors, but they have exhibited low conductivity [35]. There have been listed many studies in the literature that have conducted with various supporting materials by using transition metal oxides of MnO_2, RuO_2, Fe_2O_3, $NiCo_2O_4$, NiO, Co_3O_4 to improve low energy density and low capacitive performance of PC materials [35–40]. The energy, capacity and cycling performance of the supercapacitor can be increased by combination of PC material with metal oxides. Proper metals oxides are coated on the PC supporting material that ensures the stability of electrodes [35, 41]. Synergic effects between metal oxides and PC supporting materials (three-dimensional structure) lead to an increase in the supercapacitor performance because of increasing active sides present on the surface of PC [35].

The PC can be synthesized from various plant by a green synthesize method [42, 43]. *Astragalus* belongs to the *Fabaceae* family with more than 3000 species of small shrubs and plants. Although *Astragalus* has a wide distribution in mountainous regions, it is mostly found in the Asian continent such as Turkey, Iran, and Syria [44, 45]. *Astragalus* is a renewable, biodegradable, biocompatible, cheap, safe and natural plant [46, 47]. The roots of the *Astragalus brachycalyx* fischer plant have been used in the treatment of some ailments such as leukemia, diabetes and respiratory tract infections [48, 49]. Some *Astragalus* species like tragacanth have been used and widely studied in various applications such as stabilizer, cross-linked agents, thickener and emulsifier. Both the *Tragacanth* and *Astragalus brachycalyx* fischer structures consist of carboxylic and hydroxyl functional groups that ensure appropriate reactive sites for reagents in cross-linking [50–52].

In this study, PC as supporting materials wassuccesfully synthesized from the *Astragalus brachycalyx* fischer plant using an electronic oven under a nitrogen atmosphere. Then, $NiSnO_2$ bimetallic oxides were loaded PC according to the reduction-impregnation method [53, 54] as a straightforward process. Thus, $NiSnO_2$/PC composites were obtained and characterized by various instruments such as XRD, SEM, Raman, BET and EDS analyses. The electrode

properties of the $NiSnO_2$/PC were investigated for supercapacitor applications.

2 Experimental details

As a porous carbon source, the roots of *Astragalus brachycalyx* fischer were picked up from the border of the Ağrı in Turkey. The other chemicals such as ethylene glycol [EG, $(CH_2OH)_2$], nickel(II) chloride, polyethylene glycol [PEG, $H(OCH_2CH_2)nOH$], tin chloride ($SnCl_2{\cdot}2H_2O$), sodium hydroxide (NaOH), hydrochloric acid and nickel(II) chloride were purchased from Sigma-Aldrich. All chemicals were analytical purity and used without any purification process. The glasses such as bottles and petri dishes were cleaned with distilled water and ethanol solvents and dried at 100 °C temperature in an oven.

2.1 Synthesis of porous carbon (PC) from *Astragalus brachycalyx* fischer plant

The roots of *Astragalus brachycalyx* fischer were used as the raw material of the PC source. *Astragalus brachycalyx* fischer plants were cleaned from visible impurities and thereafter dried at 75 °C in an oven for 48 hours. The dried *Astragalus brachycalyx* fischer stems were ground into small powder particles. The carbonization experiments were performed using a pyrolysis device (Figure S1) at a rate of 5 °C/min and 600 °C temperature under nitrogen atmosphere for 60 min. The obtained solid samples were washed thoroughly by distilled water. Then, they were dried in a vacuum oven at 105 °C temperature for 24 hours. Hence, powder samples were obtained and stored for further experiments.

2.2 Synthesis of Ni/PCs

Ni-doped PC nanoparticles (Ni/PCs) were synthesized by following procedure: 10 mL solution containing 1 mmol $NiCl_2$ was prepared, and then 100 mg PC powder was added to the resulting solution. The resulting mixture was mixed for 2 hours, and 7.50 mmol (1 mL) of sodium boron hydride solution was added into the solution. The reduction process was determined by the color change. The solid samples obtained at the end of this process were filtered and washed with abundant pure water and ethyl alcohol. The solid nanoparticles were dried at 105 °C for 1 hour in an oven. The powder samples obtained were stocked in a vessel according to Ref [48].

2.3 Synthesis of $NiSnO_2$/PCs electrode materials

For the synthesis of $NiSnO_2$/PCs, a mixture of Ni/PCs (20 mg), $SnCl_2.2H_2O$ (0.88 mg) and 80 ml of deionized water were employed. This mixture was sonicated for 30 min and added into a vessel containing 10 ml of ethylene glycol at a temperature of 60 °C. Then, urea (0.20 g) and HCl (0.30 mL) were added into the solution, and the mixture was stirred for 6 hours by a magnetic stirrer. The obtained sample was thoroughly washed with deionized water and ethanol solution. The final product was then left to dry in a vacuum oven at 40 °C temperature for 24 hours according to Ref [55].

2.4 Characterizations

The carbonization experiments were carried out by DEFNE laboratory TURKEY Pyrolyse device (Figure S1) using a heating rate of 15 °C/min and temperature range of 30–600 °C (under nitrogen atmosphere). X-ray diffraction measurements of the PC and $NiSnO_2$/PC were obtained Rigaku Rint 1000 X-ray diffractometer with Cu-Ka radiation (40 kV, 40 mA). The structure and morphology characterization of the samples were achieved by a scanning electron microscope (SEM, EVO18 Germany) coupled to an energy dispersion spectrum (EDS). BET and Raman analyses were conducted by Micromeritics 3Flex Version and Renishaw inVia Raman Microscope, respectively. The cyclic voltammetry (CV) measurements were collected by Gamry Interface 1010E galvanostat/potentiostat to determine electrochemical properties.

2.5 Electrochemical performance tests

The Swagellok-type cell was used for all capacitor analyses. In order to electrode preparation of capacitors, equal amounts of PC and $NiSnO_2$/PC samples were prepared separately. Furthermore, 6 M KOH aqueous solution and the cellulosic paper were used as an electrolyte and membrane, respectively. To obtain electrochemical symmetric capacitor measurements, experiments were conducted with the

two-electrodes method. The cyclic voltammetry (CV) measurements were carried out at a constant scan speeds of 100, 200, 400 and 800 mV/s. The CV measurements were carried out as 3 cycles to observe any anomalies, but only one CV cycle datum has been given for each scanning speed in the result section to avoid data analyses confusion. The cycle life study of capacitance measurements was performed under 200 mV/s constant scanning speed in a range of 0–1 V for 200 cycles. Then, the capacitance values of the samples were calculated by Eq. 1 in the reference of CV results [56];

$$C = \frac{\int I dV}{2m\Delta V v} \quad (1)$$

where I is the current, m is the electrode active material weight, v is the scan rate and ΔV is the voltage range.

3 Results and discussion

3.1 Characterization

The XRD results of the synthesized PC and $NiSnO_2$/PC materials are given in Fig. 1 for wide range 2-theta angles. A broad peak at 23.53° can be attributed to (002) peak of the PC as shown in Fig. 1. Other PC peak at around 43–44° is not suffeciently clear because it is broad. This results a sign that carbonization of *Astragalus brachycalyx* fischer was achieved by pyrolysis device [57]. The broad peak of

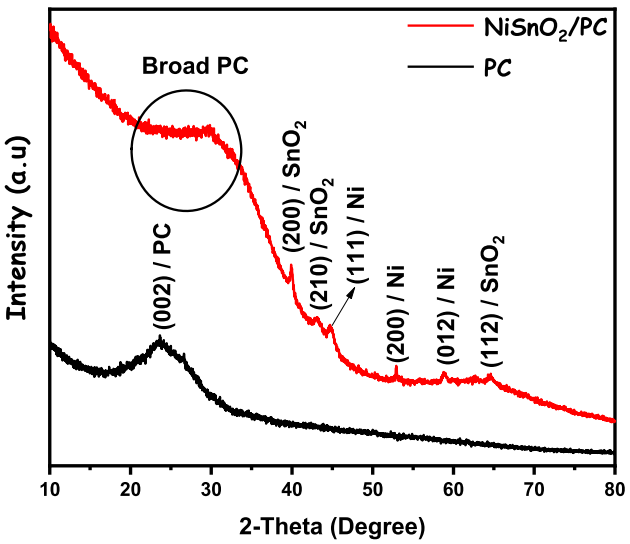

Fig. 1 XRD patterns of porous carbon and $NiSnO_2$/PC materials

PC clearly broadened and shifted toward bigger angles. However, the absence of a sharp peak that originated from carbon atoms shows forming an amorphous structure [58, 59]. The pattern of the $NiSnO_2$/PC material shows both SnO_2 and Ni peaks. The SnO_2 peaks are (200), (210) and (112), and they can be attributed to tetragonal structure of the SnO_2 according to JCPDS 41–1445 [60, 61]. XRD peaks of the Ni have been detected in the planes of (111), (200) and (012) according to the literature [62]. XRD results clearly revealed that PC and $NiSnO_2$/PC materials successfully synthesized.

SEM images for $NiSnO_2$/PC materials were conducted to detect surface variations and given in Fig. 2. SEM images obtained from different angles and at different scales show the pores in the surface structure of the PC. According to SEM analysis, it is seen that $NiSnO_2$ particles settle on the PC surface both on the surface of the PC and in the porous parts. It can be said that this affects the pore size. The addition of $NiSnO_2$ into the porous structure should also affect the conductivity.

EDS analysis results of the PC and $NiSnO_2$/PC are given in Fig. 3a and b, respectively. The existence of C and O elements was detected as 75.09% and 24.91%, respectively. The presence and percentages of Ni and Sn metals in the $NiSnO_2$/PC were proved by conducting in Fig. 4b. The presence of C, O, Ni and Sn was obtained as the percentages of the 70.61%, 26.29%, 0.95% and 0.15%, respectively. The results clearly revealed that both the PC and $NiSnO_2$/PC materials were synthesized successfully.

Figure 4 shows the Raman analysis results of the PC and $NiSnO_2$/PC materials. Raman shifts at 500–1000 cm^{-1} are various vibration modes for SnO_2. Especially, Raman shifts at 400–700 cm^{-1} are characteristic of SnO_2. Due to the expansion/contraction of the Sn–O bonds, shifts may occur in the Raman vibrations [63]. D and G Raman bands formed as a result of the addition of PC to the material structure are characteristic of carbon (ID/IG = 0.8427). The formation of D and G bands indicates that carbon has been added to the material structure. The Raman vibration band at 117 cm^{-1} is due to Ni doping. In previous studies [64], it has been reported that Raman vibration bands in the range of 100–200 cm^{-1} are formed as a result of Ni doping.

The pore properties and surface area of the material used for supercapacitors are important for capacitive efficiency. BET analysis results of $NiSnO_2$/

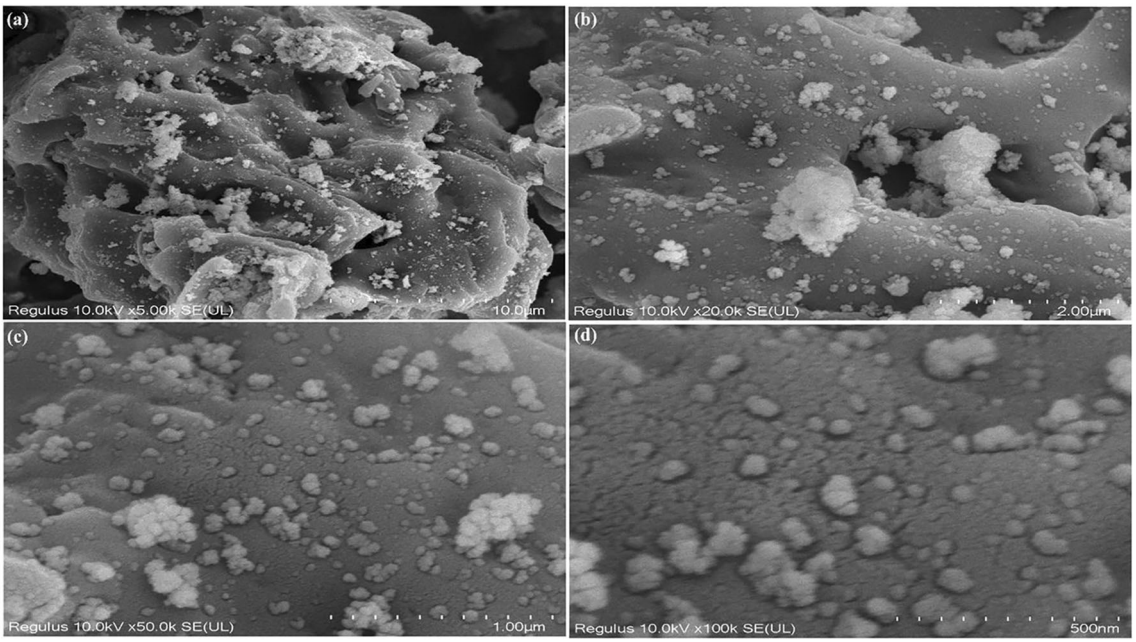

Fig. 2 SEM analyses of $NiSnO_2$/PC from different angles and sizes (**a**) 10 μm, (**b**) 2 μm, (**c**) 1 μm and (**d**) 500 nm

PC are given in Fig. 5. The surface area of $NiSnO_2$/PC is calculated as 12.64 m^2/g. The porosity formed in the material structure is due to the removal of organic substances as a result of pyrolysis in the structure of the material. However, when compared with similar porous materials [65], it is seen that there is a decrease in the number of pores and surface area. It can be said that the addition of $NiSnO_2$ to the PC structure causes a decrease in the pore number and surface area.

3.2 Electrochemical analysis

Figure 6a and b show the CV analysis results of the symmetric capacitors formed with PC and $NiSnO_2$/PC active materials. The CV patterns show that both materials have permanent capacitive current flats in the ± 1 V range. Under normal conditions, permanent flats of capacitive currents are expected result for both carbon-based materials. However, another remarkable situation in CV patterns is that the current values obtained in the $NiSnO_2$/PC structure (after ~ 0.50 V value) are higher than the PC structure. This situation led to question the possible presence of redox with $NiSnO_2$.

For $NiSnO_2$/PC samples, the bumps formed on the CV curves indicate possible redox peak formations, while the first-order derivative of the current will help to understand this situation more clearly by considering the voltage in the CV analysis. With this calculation, the maximum/minimum values that will emerge and the starting and ending voltage values of possible redox peaks will be able to be determined. The redox peak voltage values for the $NiSnO_2$/PC electrode materials are given in Fig. 7. According to the dI/dV calculation, it was determined that the oxidation reactions and these reactions reached their peak at 0.46 V for both 100 and 200 mV/s scan rate and 0.51 V and 0.65 V for 400 and 800 mV/s, respectively. A literature survey was conducted to understand which atom/atoms or molecules that caused these oxidation reactions. Similar redox reactions were observed in the study of Pascariu et al. [66]. In this study, while no oxidation reaction was observed with SnO_2/polythiophene in the 0-1 V range, it was determined that oxidation peaks occurred in the 0–1 V range with Ni doping to SnO_2/polythiophene. This situation suggests that the oxidation peaks may belong to Ni metals in $NiSnO_2$/PC. In addition, Ni-doped nano-PC particles may cause these oxidation reactions. The amorphous structure formed in the $NiSnO_2$/PC structure may also be another source of these oxidation reactions.

Another important point is that there are shifts in the oxidation peaks at increasing voltage scan speeds after 200 mV/s. The main reason may be more voltage is needed to ensure ionic transfer in the structure

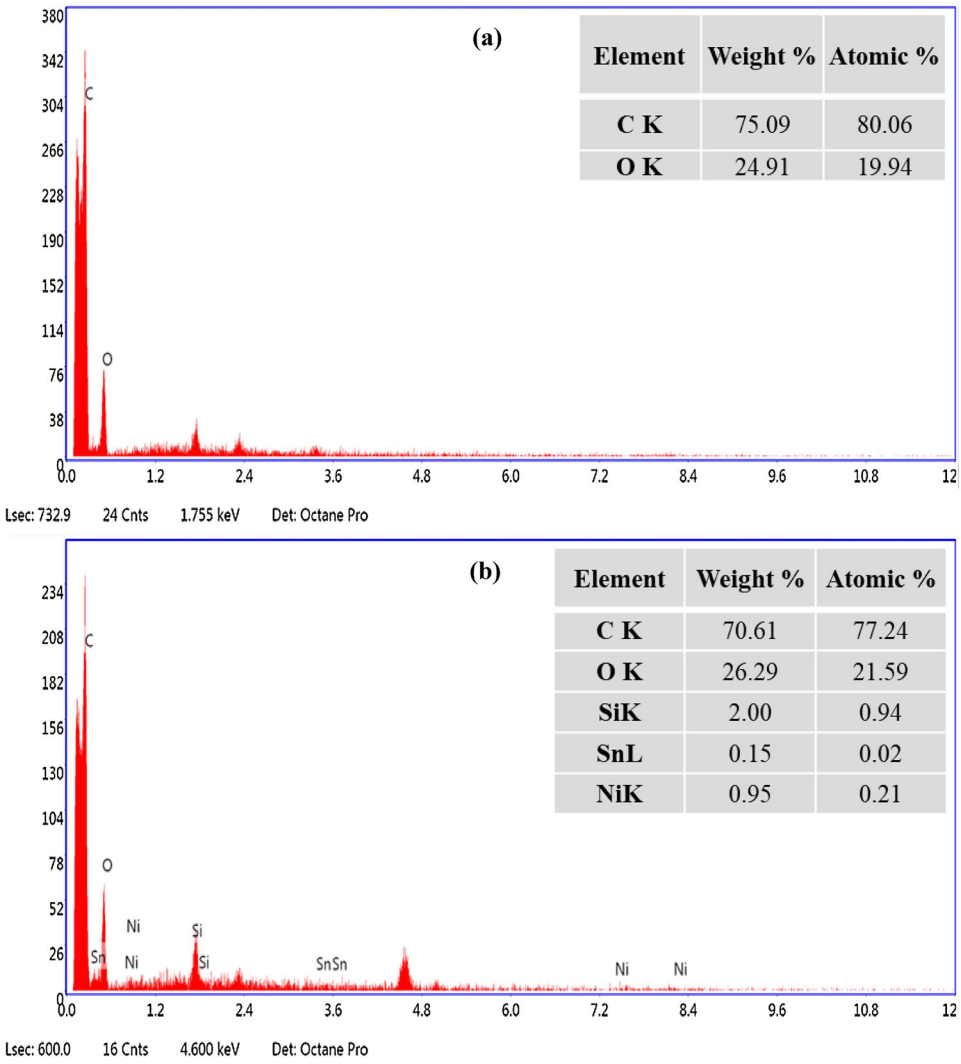

Element	Weight %	Atomic %
C K	75.09	80.06
O K	24.91	19.94

Element	Weight %	Atomic %
C K	70.61	77.24
O K	26.29	21.59
SiK	2.00	0.94
SnL	0.15	0.02
NiK	0.95	0.21

Fig. 3 EDS spectrum of (**a**) PC and (**b**) $NiSnO_2$/PC

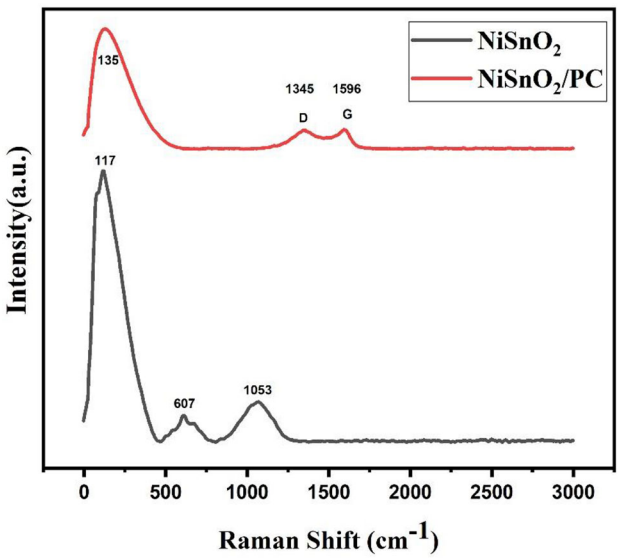

Fig. 4 Raman analyses of NiSnO2 and $NiSnO_2$/PC

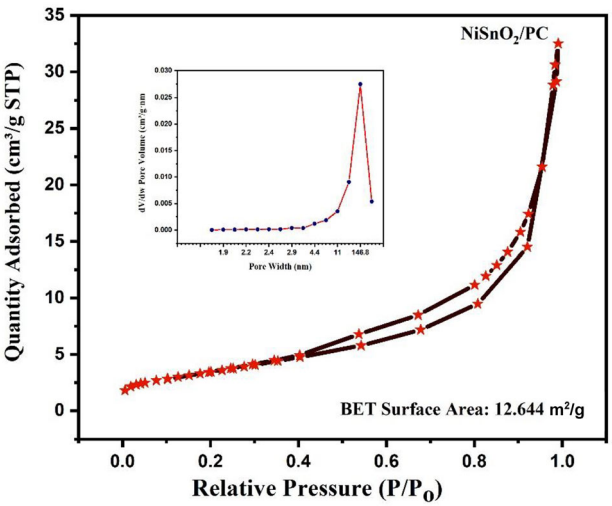

Fig. 5 BET analysis of $NiSnO_2$/PC

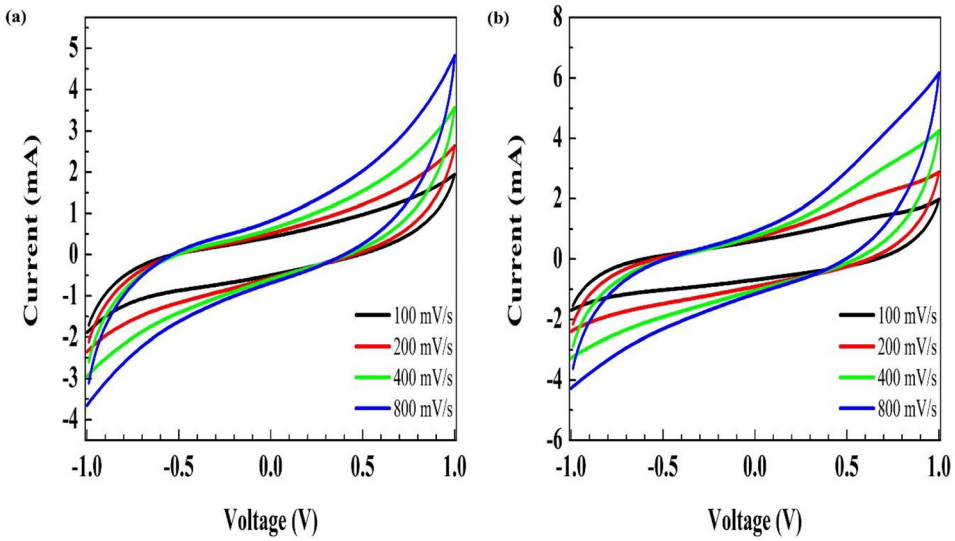

Fig. 6 Cyclic voltammetry analyses of (**a**) PC and (**b**) $NiSnO_2$/PC electrodes

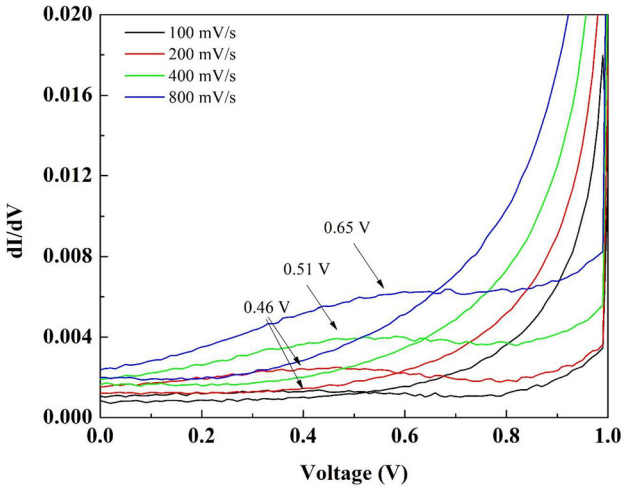

Fig. 7 dI/dV analysis of $NiSnO_2$/PC electrodes

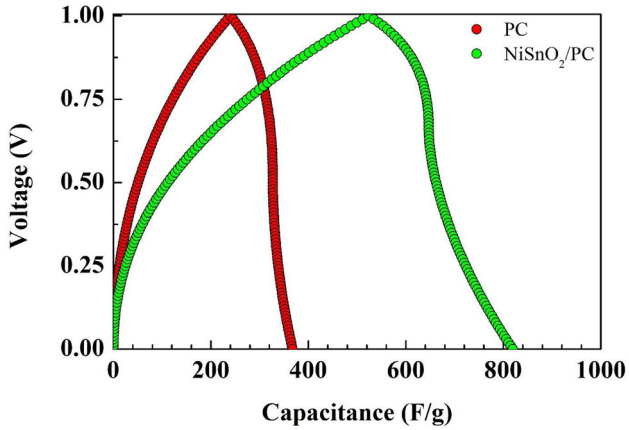

Fig. 8 First-cycle analysis of PC and $NiSnO_2$/PC symmetric capacitors

during the rapid charge–discharge process [67]. In other words, this indicates that there are some problems in ionic diffusion (such as diffusion pathway changes, ion aggregation, ion bond or ion impurity interactions) within the $NiSnO_2$/PC structure.

Figure 8 shows the first charge–discharge cycle measurement results of symmetric capacitors prepared with PC and $NiSnO_2$/PC electrodes, separately. Especially, the redox reactions determined in Fig. 8 are easily seen in the discharge pattern obtained at the end of the first cycle. The $NiSnO_2$/PC electrodes have higher capacitance than pure PC capacitors in the range of 0.50–1 V. While a charge capacitance was ~ 239 F/g with PC symmetric capacitors, a discharge capacitance was obtained as ~ 127 F/g between 0 and 1 V. In the case of $NiSnO_2$/PC symmetric capacitors, these values were measured as ~ 522 F/g charges and ~ 296 F/g discharge capacitance. With the doping of $NiSnO_2$ to the PC structure, the capacitances increased more than 2 times. Considering the SEM analysis, it was observed that the particle size increased and the pore number decreased with the doping of $NiSnO_2$. The increase in the particle sizes causes a decrease in the surface area of the material, and it may show that this situation can cause a possible decrease in capacitance because the higher surface area provides higher level electrolyte–electrode interaction and higher amount ion moves. However, the obtained results revealed that the $NiSnO_2$ doping was effective for providing possible vibration stabilization in the particles. Moreover, $NiSnO_2$ doping can provide capacitive

increase due to redox reactions [53]. During the charge–discharge reactions, vibrations occur in the bond structures during the diffusion of ions (K^+ or O^-) towards the electrodes, and these vibrations may prevent the ion diffusion and ion binding to the electrodes for greater amounts. Therefore, the stable performance of the bond or crystal structures of the electrodes may affect the capacitive performance of the capacitors.

Figure 8 shows the capacitive performances of PC and $NiSnO_2$/PC capacitors depending on the cycle life. The capacitance superiority of $NiSnO_2$/PC electrodes over PC electrodes continued during 200 charge–discharge cycles. When the results are analyzed statistically, charge–discharge capacitance values can continue for similar values during longer cycles. Table 1 shows the charge and discharge capacitance values of some specific cycles. The capacity retention values of the capacitors were calculated according to these specific capacitance values. Capacity retention formula is given by:

$$Retention(\%) = \frac{C_0 - C_n}{C_0} \times 100 \quad (2)$$

where C_0 is the first-cycle capacitance value (F/g) and C_n is the last cycle capacitance (F/g).

When Fig. 9 and Table1 are evaluated together, the capacitance loss of 71.48% for charge and 45.55% for discharge occurs in PC capacitors at the end of 200 cycles. $NiSnO_2$/PC capacitors have the capacitance loss of 61.75% for charging and 38.70% for discharge. This value shows that $NiSnO_2$/PC electrodes are good for supercapacitor applications. Especially evaluation of Fig. 9, it was determined that the stable atomic behaviors formed in the electrode active material also affected the cycle life of the capacitors. Similar to the our study, Liu et al. were determined that high-performance energy storage systems obtained in terms of cycle life with electrode stabilization [68]. As a result, the stabilization effect is

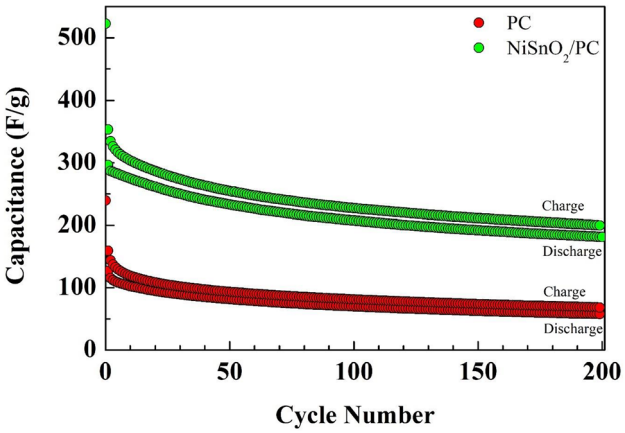

Fig. 9 Cycle life performance of PC and $NiSnO_2$/PC symmetric supercapacitors

created by the $NiSnO_2$ doping into PC structure, and it created positive results in terms of both capacitive and cycle life. Another explanation is may under normal conditions, the obtained Coulomb Efficiency (CE) was close to 100% in carbon-based electrodes, while this situation was lower in the NiSnO2/PC structure. Since the cathodic-anodic behavior of the electrodes can directly affect the electrolyte polarization, especially with the application of symmetrical capacitors, the decrease in CE values at these levels is not surprising.

In the last stage of our study, the capacitance levels of some specific symmetric capacitors with different electrode materials were compared. Table 2 displays the comparison of this study with some of previous studies except for carbon nanofiber (CNF) and NiO structures. The metal oxide structures generally provide lower capacitance than carbon-based capacitors. When the capacitance performances are compared of these materials with the PC materials we produced, the PC structure provides better capacitance values. The PC can increase the electric field size of capacitors with the higher surface area of the electrodes and more ion diffusion. Furthermore, the higher

Table 1 Capacitance and capacity retention values of capacitors

Material	1. cycle		50. cycle		100. cycle		200. cycle		Retention (%)	
	Ch	Dch	Ch	Dch	Ch	Dch	Ch	Dch	Ch	Dch
PC	239.50	127.10	93.70	81.74	81.30	70.10	68.30	57.90	71.48	45.55
$NiSnO_2$/PC	522.60	295.90	255.50	233.10	227.80	207.60	199.90	181.40	61.75	38.70

Ch charge capacitance (F/g); *Dch* discharge capacitance (F/g)

Table 2 Some electrode materials are fabricated using carbon-based and metal oxide-based materials for use in supercapacitors

Number	Electrode materials	Capacitor type	Discharge capacitance (F/g)	Refererance
1	CNF	Symmetric	19	[68]
2	AC	Symmetric	90–110	[69]
3	NiO	Symmetric	161	[70]
4	NiOH	Symmetric	78	[71]
5	MnO_2	Symmetric	85	[72]
6	PC	Symmetric	127.10	This study
7	$NiSnO_2$/PC	Symmetric	295.90	This study

CNF carbon nanofibers; *AC* activated carbon

capacitance levels can be achieved by much more porous structures amounts. On the other hand, in metal oxide structures, a discharge capacitance of 85 F/g was obtained with MnO_2, and a capacitance of 161 F/g was achieved with NiO. According to these capacitance values, the connection of the PC and $NiSnO_2$ structures with each other was demonstrated much more capacitance values according to this study. The highest capacitance performance has been obtained by 295.90 F/g discharge capacitance with the $NiSnO_2$/PC electrodes, and they are suitable for industrial supercapacitors applications.

In the scope of the study, the energy (E) and power (P) densities were also calculated depending on charge and discharge capacitance values by (3) and (4) equations [73].

$$E = \frac{1}{2} \times C \times \Delta V^2 \times \frac{1}{3.6} \tag{3}$$

$$P = \frac{E}{t} \times 3600 \tag{4}$$

where C is the capacitance (F), ΔV is the potential window, and t is the time. When the energy and power density amounts are calculated from the capacitance values, according to the $NiSnO_2$/PC capacitance results, an energy density of 73.16 Wh/kg and a power density of 52.68 kW/kg are obtained in charge. In case of discharge, 41.43 Wh/kg energy density and 29.83 kW/kg power density are provided. On the other hand, these values are, according to PC materials, the charge capacitance values; it corresponds to an energy density of 33.53 Wh/kg and a power density of 24.14 kW/kg. In case of discharge, an energy density of 17.79 Wh/kg and a power density of 12.81 kW/kg are obtained. As a result of energy and power densities calculations, it has been discovered that NiSnO2-doped PC materials can store higher power and energy.

4 Conclusion

In this study, $NiSnO_2$/PC anodic materials were synthesized and characterized, and their supercapacitor features were investigated by applying cyclic voltammetry analysis, dI/dV analysis and capacitive performances. PC was obtained using *Astragalus brachycalyx* fischer plant as cheap materials using pyrolyzes devices under nitrogen atmosphere. PC and $NiSnO_2$/PC characterizations were carried out by XRD, SEM, EDS, Raman and BET analyses techniques. SEM analyses showed the porous structure of PC and porous of the PC diminished with the $NiSnO_2$/PC. In addition, EDS analyses were confirmed the present Ni, Sn, C and O elements in the structure of $NiSnO_2$/PC. Raman results confirmed vibration of SnO_2 modes, Ni doping vibraton and carbon bands. BET analysis of $NiSnO_2$/PC revealed 12.64 m^2/g surface area and porosity. The CV results confirmed the permanent capacitive plains for both materials. Moreover, $NiSnO_2$ doping caused some redox reactions in capacitor applications. Although the surface area and pore content decreased with doping, the possible structural stabilization obtained with $NiSnO_2$ resulted in a more than 2 times increase in capacitance performance. The electrochemical studies revealed that the $NiSnO_2$/PC active materials exhibited 295.90 F/g discharge capacitance as a supercapacitor. This result also promises that $NiSnO_2$/PC active materials can be used as high-performance electrode materials in industrial production.

Author contributions

SD contributed to investigation, methodology, data curation and writing original draft. MSN contributed

to investigation, synthesis, methodology and data curation. AK contributed to data curation, writing—reviewing and editing. MHC contributed to investigation, synthesis, methodology and writing original draft. MHA contributed to writing—reviewing and editing.

Funding

The authors have not disclosed any funding.

Data availability

Data are available upon reasonable request.

Declarations

Conflict of interest The authors declare no conflict of interest.

Supplementary Information: The online version contains supplementary material available at https://doi.org/10.1007/s10854-023-09894-7.

References

1. A. González, E. Goikolea, J.A. Barrena, R. Mysyk, Review on supercapacitors: technologies and materials. Renew. Sustain. Energy Rev. **58**, 1189–1206 (2016). https://doi.org/10.1016/J.RSER.2015.12.249
2. K. Aruchamy, R. Nagaraj, H.M. Manohara, M.R. Nidhi, D. Mondal, D. Ghosh, S.K. Nataraj, One-step green route synthesis of spinel $ZnMn_2O_4$ nanoparticles decorated on MWCNTs as a novel electrode material for supercapacitor. Mater. Sci. Eng. B. (2020). https://doi.org/10.1016/J.MSEB.2019.114481
3. J. Bhagwan, S.K. Hussain, B.N.V. Krishna, J.S. Yu, Facile synthesis of $MnMoO_4$@MWCNT and their electrochemical performance in aqueous asymmetric supercapacitor. J. Alloys Compd. (2021). https://doi.org/10.1016/J.JALLCOM.2020.157874
4. A.M. Abioye, F.N. Ani, Recent development in the production of activated carbon electrodes from agricultural waste biomass for supercapacitors: a review. Renew. Sustain. Energy Rev. **52**, 1282–1293 (2015). https://doi.org/10.1016/J.RSER.2015.07.129
5. S. Dühnen, J. Betz, M. Kolek, R. Schmuch, M. Winter, T. Placke, Toward green battery cells: perspective on materials and technologies. Small Methods. **4**, 2000039 (2020). https://doi.org/10.1002/smtd.202000039
6. A. Kausar, Green nanocomposites for energy storage. J. Compos. Sci. **5**, 202 (2021). https://doi.org/10.3390/jcs5080202
7. Y. Ma, X. Xie, W. Yang, Z. Yu, X. Sun, Y. Zhang, X. Yang, H. Kimura, C. Hou, Z. Guo, W. Du, Recent advances in transition metal oxides with different dimensions as electrodes for high-performance supercapacitors. Adv. Compos. Hybrid Mater. **4**, 906–924 (2021). https://doi.org/10.1007/s42114-021-00358-2
8. Z. Li, C. Wang, F. Ling, L. Wang, R. Bai, Y. Shao, Q. Chen, H. Yuan, Y. Yu, Y. Tan, Room-temperature sodium-sulfur batteries: rules for catalyst selection and electrode design. Adv. Mater. **34**, 2204214 (2022). https://doi.org/10.1002/adma.202204214
9. A.I.M. Albashir, W. Shang, M.K. Hadi, J. Zhang, T. Zhang, F. Ran, Straightforward solution polymerization synthesis of porous carbon@gold nanoparticles electrode for high-performance supercapacitor. J. Energy Storage. (2021). https://doi.org/10.1016/J.EST.2020.102041
10. F. Ran, K. Shen, Y. Tan, B. Peng, S. Chen, W. Zhang, X. Niu, L. Kong, L. Kang, Activated hierarchical porous carbon as electrode membrane accommodated with triblock copolymer for supercapacitors. J. Memb. Sci. **514**, 366–375 (2016). https://doi.org/10.1016/J.MEMSCI.2016.05.011
11. K.V.G. Raghavendra, R. Vinoth, K. Zeb, C.V.V. Muralee Gopi, S. Sambasivam, M.R. Kummara, I.M. Obaidat, H.J. Kim, An intuitive review of supercapacitors with recent progress and novel device applications. J. Energy Storage. (2020). https://doi.org/10.1016/J.EST.2020.101652
12. G. Huang, Q. Geng, W. Kang, Y. Liu, Y. Li, B. Xing, Q. Liu, C. Zhang, Hierarchical porous carbon with optimized mesopore structure and nitrogen doping for supercapacitor electrodes. Microporous Mesoporous Mater (2019). https://doi.org/10.1016/J.MICROMESO.2019.109576
13. X. Zhao, G. Nie, Y. Luan, X. Wang, S. Yan, Y.Z. Long, Nitrogen-doped carbon networks derived from the electrospun polyacrylonitrile@branched polyethylenimine nanofibers as flexible supercapacitor electrodes. J. Alloys Compd. (2019). https://doi.org/10.1016/J.JALLCOM.2019.151737
14. X. Li, D. Du, Y. Zhang, W. Xing, Q. Xue, Z. Yan, Layered double hydroxides toward high-performance supercapacitors. J. Mater. Chem. A. **5**, 15460–15485 (2017). https://doi.org/10.1039/C7TA04001F
15. H. Wang, Z. Xu, A. Kohandehghan, Z. Li, K. Cui, X. Tan, T.J. Stephenson, C.K. King'Ondu, C.M. Holt, B.C. Olsen, J.K. Tak, D. Harfield, A.O. Anyia, D. Mitlin, Interconnected

carbon nanosheets derived from hemp for ultrafast supercapacitors with high energy. ACS Nano **7**(6), 5131–5141 (2013). https://doi.org/10.1021/NN400731G

16. M. Zhi, C. Xiang, J. Li, M. Li, N. Wu, Nanostructured carbon–metal oxide composite electrodes for supercapacitors: a review. Nanoscale **5**, 72–88 (2012). https://doi.org/10.1039/C2NR32040A
17. J. Jiang, Y. Li, J. Liu, X. Huang, C. Yuan, X.W. Lou, Recent advances in metal oxide-based electrode architecture design for electrochemical energy storage. Adv. Mater. **24**, 5166–5180 (2012). https://doi.org/10.1002/ADMA.201202146
18. L.Z.J.Z.G. Wang, A review of electrode materials for electrochemical supercapacitors. Chem. Soc. Rev. **41**, 797–828 (2012). https://doi.org/10.1039/c1cs15060j
19. J. Li, Y. Gao, K. Han, J. Qi, M. Li, Z. Teng, High performance hierarchical porous carbon derived from distinctive plant tissue for supercapacitor. Sci. Rep. **9**, 1–11 (2019). https://doi.org/10.1038/s41598-019-53869-w
20. Y. Wang, C. Lu, X. Cao, Q. Wang, G. Yang, J. Chen, Porous carbon spheres derived from hemicelluloses for supercapacitor application. Int. J. Mol. Sci. **23**, 7101 (2022). https://doi.org/10.3390/ijms23137101
21. Y. Zhao, Z. Yang, W. Fan, Y. Wang, G. Li, H. Cong, H. Yuan, Carbon nanotube/carbon fiber electrodes via chemical vapor deposition for simultaneous determination of ascorbic acid, dopamine and uric acid. Arab. J. Chem. **13**, 3266–3275 (2020). https://doi.org/10.1016/j.arabjc.2018.11.002
22. G. Li, H. Yuan, J. Mou, E. Dai, H. Zhang, Z. Li, Y. Zhao, Y. Dai, X. Zhang, Electrochemical detection of nitrate with carbon nanofibers and copper co-modified carbon fiber electrodes. Compos. Commun. (2022). https://doi.org/10.1016/j.coco.2021.101043
23. Y. Lei, R. Huang, L. Guo, H. Xie, D. Zhang, M. Li, Effect of activating agents on the structure and capacitance performance of tofu derived porous carbon. J. Mater. Sci. Mater. Electron. **30**(11), 10274–10283 (2019). https://doi.org/10.1007/S10854-019-01364-3
24. Y. Tan, Y. Liu, L. Kong, L. Kang, C. Xu, F. Ran, In situ doping of PANI nanocomposites by gold nanoparticles for high-performance electrochemical energy storage. J. Appl. Polym. Sci. (2017). https://doi.org/10.1002/APP.45309
25. C. Liu, Z. Yu, D. Neff, A. Zhamu, B.Z. Jang, Graphene-based supercapacitor with an ultrahigh energy density. Nano Lett. **10**, 4863–4868 (2010). https://doi.org/10.1021/NL102661Q
26. J. Tao, N. Liu, W. Ma, L. Ding, L. Li, J. Su, Y. Gao, Solid-state high performance flexible supercapacitors based on polypyrrole-MnO_2-carbon fiber hybrid structure. Sci Rep (2013). https://doi.org/10.1038/SREP02286
27. J. Tian, T. Zhang, D. Talifu, A. Abulizi, Y. Ji, Porous carbon materials derived from waste cotton stalk with ultra-high surface area for high performance supercapacitors. Mater. Res. Bull. (2021). https://doi.org/10.1016/J.MATERRESBULL.2021.111457
28. J. Du, L. Liu, Z. Hu, Y. Yu, Y. Zhang, S. Hou, A. Chen, Raw-cotton-derived N-doped carbon fiber aerogel as an efficient electrode for electrochemical capacitors. ACS Sustain. Chem. Eng. **6**, 4008–4015 (2018). https://doi.org/10.1021/ACSSUSCHEMENG.7B04396
29. A.A. Mohammed, C. Chen, Z. Zhu, Low-cost, high-performance supercapacitor based on activated carbon electrode materials derived from baobab fruit shells. J. Colloid Interface Sci. **538**, 308–319 (2019). https://doi.org/10.1016/J.JCIS.2018.11.103
30. P. Liu, Y. Wen, L. Huang, X. Zhu, R. Wu, S. Ai, T. Xue, Y. Ge, An emerging machine learning strategy for the assisted-design of high-performance supercapacitor materials by mining the relationship between capacitance and structural features of porous carbon. J. Electroanal. Chem. (2021). https://doi.org/10.1016/J.JELECHEM.2021.115684
31. H. He, Y. Zhang, P. Wang, D. Hu, Preparation of sponge-cake-like N-doped porous carbon materials derived from silk fibroin by chemical activation. Microporous Mesoporous Mater. (2021). https://doi.org/10.1016/J.MICROMESO.2021.110998
32. J. Chen, L. Jiang, W. Wang, P. Wang, X. Li, H. Ren, Y. Wang, Facile construction of highly porous carbon materials derived from porous aromatic frameworks for greenhouse gas adsorption and separation. Microporous Mesoporous Mater. (2021). https://doi.org/10.1016/J.MICROMESO.2021.111385
33. S. Liu, X. Hu, J. Ma, M. Li, H. Lin, S. Han, N/P codoped carbon materials with an ultrahigh specific surface area and hierarchical porous structure derived from durian peel for high-performance supercapacitors. Energy Fuels **34**, 14948–14957 (2020). https://doi.org/10.1021/ACS.ENERGYFUELS.0C02682
34. H. Zhou, R. Shu, F. Guo, J. Bai, Y. Zhan, Y. Chen, L. Qian, N–O–P co-doped porous carbon aerogel derived from low-cost biomass as electrode material for high-performance supercapacitors. Diam. Relat. Mater. (2021). https://doi.org/10.1016/J.DIAMOND.2021.108614
35. R. Wang, X. Li, Z. Nie, Y. Zhao, H. Wang, Metal/metal oxide nanoparticles-composited porous carbon for high-performance supercapacitors. J. Energy Storage. (2021). https://doi.org/10.1016/J.EST.2021.102479
36. C. Liu, J. Li, J. Qi, J. Wang, R. Luo, J. Shen, X. Sun, W. Han, L. Wang, Yolk-shell Fe0@SiO_2 nanoparticles as nanoreactors for fenton-like catalytic reaction. ACS Appl. Mater.

Interfaces. **6**, 13167–13173 (2014). https://doi.org/10.1021/AM503063M

37. R. Guan, L. Zhong, S. Wang, D. Han, M. Xiao, L. Sun, Y. Meng, Synergetic covalent and spatial confinement of sulfur species by phthalazinone-containing covalent triazine frameworks for ultrahigh performance of Li-S batteries. ACS Appl. Mater. Interfaces. **12**, 8296–8305 (2020). https://doi.org/10.1021/ACSAMI.9B21481
38. L. Zhong, Y. Mo, K. Deng, S. Wang, D. Han, S. Ren, M. Xiao, Y. Meng, Lithium borate containing bifunctional binder to address both ion transporting and polysulfide trapping for high-performance Li-S batteries. ACS Appl. Mater. Interfaces. **11**, 28968–28977 (2019). https://doi.org/10.1021/ACSAMI.9B09604
39. S. Zhou, T. Mei, J. Liu, X. Wang, Y. Qian, Hierarchical fusiform microrods constructed by parallelly arranged nanoplatelets of $LiCoO_2$ material with ultrahigh rate performance. ACS Appl. Mater. Interfaces. **12**, 17376–17384 (2020). https://doi.org/10.1021/ACSAMI.9B21526
40. B. Zhang, M. Xiao, S. Wang, D. Han, S. Song, G. Chen, Y. Meng, Novel hierarchically porous carbon materials obtained from natural biopolymer as host matrixes for lithium-sulfur battery applications. ACS Appl. Mater. Interfaces. **6**, 13174–13182 (2014). https://doi.org/10.1021/AM503069J
41. M. Zhi, C. Xiang, J. Li, M. Li, Wu. Nianqiang, Nanostructured carbon–metal oxide composite electrodes for supercapacitors: a review. Nanoscale **5**, 72–88 (2012). https://doi.org/10.1039/C2NR32040A
42. Y. Cheng, L. Wu, C. Fang, T. Li, J. Chen, M. Yang, Q. Zhang, Synthesis of porous carbon materials derived from laminaria japonica via simple carbonization and activation for supercapacitors. J. Mater. Res. Technol. **9**, 3261–3271 (2020). https://doi.org/10.1016/j.jmrt.2020.01.022
43. H.A. Hamouda, S. Cui, X. Dai, L. Xiao, X. Xie, H. Peng, G. Ma, Synthesis of porous carbon material based on biomass derived from hibiscus sabdariffa fruits as active electrodes for high-performance symmetric supercapacitors. RSC Adv. **11**, 354–363 (2020). https://doi.org/10.1039/d0ra09509e
44. M. Ranjbar, R. Karamian, Astragalus sect. Astragalus (Fabaceae) in Iran, complementary notes with a key to the species. Nord. J. Bot. **22**(2), 177–182 (2002). https://doi.org/10.1111/J.1756-1051.2002.TB01363.X
45. B. Aslanipour, D. Gülcemal, A. Nalbantsoy, H. Yusufoglu, E. Bedir, Cycloartane-type glycosides from *Astragalus brachycalyx* FISCHER and their effects on cytokine release and hemolysis. Phytochem. Lett. **21**, 66–73 (2017). https://doi.org/10.1016/J.PHYTOL.2017.05.028
46. M. Nejatian, S. Abbasi, F. Azarikia, Gum tragacanth: structure, characteristics and applications in foods. Int. J. Biol. Macromol. **160**, 846–860 (2020). https://doi.org/10.1016/J.IJBIOMAC.2020.05.214
47. S. Mallakpour, F. Tabesh, Green and plant-based adsorbent from tragacanth gum and carboxyl-functionalized carbon nanotube hydrogel bionanocomposite for the super removal of methylene blue dye. Int. J. Biol. Macromol. **166**, 722–729 (2021). https://doi.org/10.1016/J.IJBIOMAC.2020.10.229
48. Z. Talaei, A.R. Mahjoub, M.M. Eskandari, A.M. 2010 Rashidi, Effect of carboxylic acid salts on the syntheses of Pt/MWNTs for nitrobenzene hydrogenation, Proc. - 2010 8th Int. Vac. Electron Sources Conf. Nanocarbon, IVESC 2010 NANOcarbon Doi: https://doi.org/10.1109/IVESC.2010.5644286.
49. H. Demiral, C. Güngör, Adsorption of copper(II) from aqueous solutions on activated carbon prepared from grape bagasse. J. Clean. Prod. **124**, 103–113 (2016). https://doi.org/10.1016/J.JCLEPRO.2016.02.084
50. F. Chenlo, R. Moreira, C. Silva, Rheological behaviour of aqueous systems of tragacanth and guar gums with storage time. J. Food Eng. **96**, 107–113 (2010). https://doi.org/10.1016/J.JFOODENG.2009.07.003
51. S. Balaghi, M.A. Mohammadifar, A. Zargaraan, Physicochemical and rheological characterization of gum tragacanth exudates from six species of iranian astragalus. Food Biophys. **5**, 59–71 (2010). https://doi.org/10.1007/S11483-009-9144-5
52. S. Ghayempour, M. Montazer, M. Mahmoudi Rad, Tragacanth gum as a natural polymeric wall for producing antimicrobial nanocapsules loaded with plant extract. Int. J. Biol. Macromol. **81**, 514–520 (2015). https://doi.org/10.1016/J.IJBIOMAC.2015.08.041
53. M.H. Çalımlı, Magnetic nanocomposite cobalt-multiwalled carbon nanotube and adsorption kinetics of methylene blue using an ultrasonic batch. Int. J. Environ. Sci. Technol. (2020). https://doi.org/10.1007/s13762-020-02855-1
54. K. Karakas, A. Celebioglu, M. Celebi, T. Uyar, M. Zahmakiran, Nickel nanoparticles decorated on electrospun polycaprolactone/chitosan nanofibers as flexible, highly active and reusable nanocatalyst in the reduction of nitrophenols under mild conditions. Appl. Catal. B Environ. **203**, 549–562 (2017). https://doi.org/10.1016/J.APCATB.2016.10.020
55. S. Navazani, M. Hassanisadi, M.M. Eskandari, Z. Talaei, Design and evaluation of SnO_2-Pt/MWCNTs hybrid system as room temperature-methane sensor. Synth. Met. (2020). https://doi.org/10.1016/J.SYNTHMET.2019.116267
56. K. Cicek, S. Demirel, Self-healable PVA–graphite–borax as electrode and electrolyte properties for smart and flexible supercapacitor applications. J. Mater. Sci. Mater. Electron. **32**,

16335–16345 (2021). https://doi.org/10.1007/s10854-021-06186-w
57. K.J. Lee, E.J. Yi, Y. Kang, H. Hwang, A novel method of silicon carbide coating to protect porous carbon against oxidation. Int. J. Refract. Met. Hard Mater. (2021). https://doi.org/10.1016/J.IJRMHM.2021.105596
58. Z. Zhu, S. Wang, J. Du, Q. Jin, T. Zhang, F. Cheng, J. Chen, Ultrasmall sn nanoparticles embedded in nitrogen-doped porous carbon as high-performance anode for lithium-ion batteries. Nano Lett. **14**, 153–157 (2013). https://doi.org/10.1021/NL403631H
59. K. Liu, J. Wang, H. Zheng, X. Sun, Z. Yang, J. Man, X. Wang, J. Sun, Direct synthesis of tin spheres/nitrogen-doped porous carbon composite by self-formed template method for enhanced lithium storage. J. Mater. Sci. Technol. **104**, 88–97 (2022). https://doi.org/10.1016/J.JMST.2021.06.054
60. K.S. Yoo, S.D. Han, H.G. Moon, S.J. Yoon, C.Y. Kang, Highly sensitive H_2S sensor based on the metal-catalyzed SnO_2 nanocolumns fabricated by glancing angle deposition. Sensors **15**(7), 15468–15477 (2015). https://doi.org/10.3390/S150715468
61. W. Chen, D. Ghosh, S. Chen, Large-scale electrochemical synthesis of SnO_2 nanoparticles. J. Mater. Sci. **43**, 5291–5299 (2008). https://doi.org/10.1007/s10853-008-2792-x
62. T.Y. Yung, L.Y. Huang, T.Y. Chan, K.S. Wang, T.Y. Liu, P.T. Chen, C.Y. Chao, L.K. Liu, Synthesis and characterizations of Ni-NiO nanoparticles on PDDA-modified graphene for oxygen reduction reaction. Nanoscale Res. Lett. **9**, 1–6 (2014). https://doi.org/10.1186/1556-276X-9-444
63. P. Srinivasa Subbarao, Y. Aparna, K.L. Chitturi, Synthesis and characterization of Ni doped SnO_2 nanoparticles by sol-gel method for novel applications. Mater. Today Proc. **26**, 1676–1680 (2020). https://doi.org/10.1016/J.MATPR.2020.02.353
64. X. Lin, M.H. Rümmeli, T. Gemming, T. Pichler, D. Valentin, G. Ruani, C. Taliani, Single-wall carbon nanotubes prepared with different kinds of Ni–Co catalysts: Raman and optical spectrum analysis. Carbon N. Y. **45**, 196–202 (2007). https://doi.org/10.1016/J.CARBON.2006.06.022
65. X. Liu, Q. Li, Y. Cui, J. Lin, L. Ding, Synthesis of porous spherical ZnO nanomaterials and the selective detection of NO at room temperature. Sensors Actuators B Chem (2023). https://doi.org/10.1016/J.SNB.2022.133155
66. P. Pascariu, I.V. Tudose, D. Vernardou, E. Koudoumas, O.N. Ionescu, S. Bucur, M. Suchea, SnO_2 and Ni doped SnO_2 / polythiophene nanocomposites for gas sensing applications, Solid State. Electron. Lett. **2**, 85–91 (2020). https://doi.org/10.1016/J.SSEL.2020.11.003
67. S.R. Ede, S. Anantharaj, K.T. Kumaran, S. Mishra, S. Kundu, One step synthesis of $Ni/Ni(OH)_2$ nano sheets (NSs) and their application in asymmetric supercapacitors. RSC Adv. **7**, 5898–5911 (2017). https://doi.org/10.1039/c6ra26584g
68. A. Daraghmeh, S. Hussain, I. Saadeddin, L. Servera, E. Xuriguera, A. Cornet, A. Cirera, Study of carbon nanofibers and active carbon as symmetric supercapacitor in aqueous electrolyte: a comparative study. Nanoscale Res. Lett. (2017). https://doi.org/10.1186/S11671-017-2415-Z
69. Q. Abbas, D. Pajak, E. Frąckowiak, F. Béguin, Effect of binder on the performance of carbon/carbon symmetric capacitors in salt aqueous electrolyte. Electrochim. Acta. **140**, 132–138 (2014). https://doi.org/10.1016/J.ELECTACTA.2014.04.096
70. C.-S. Kwak, T.H. Ko, J.H. Lee, H.-Y. Kim, B.-S. Kim, Flexible transparent symmetric solid-state supercapacitors based on NiO-decorated nanofiber-based composite electrodes with excellent mechanical flexibility and cyclability. ACS Appl. Energy Mater. **3**, 2394–2403 (2020). https://doi.org/10.1021/ACSAEM.9B02073
71. H. Du, Y. Pan, X. Zhang, F. Cao, T. Wan, H. Du, R. Joshi, D. Chu, Silver nanowire/nickel hydroxide nanosheet composite for a transparent electrode and all-solid-state supercapacitor. Nanoscale Adv. **1**, 140–146 (2019). https://doi.org/10.1039/C8NA00110C
72. G.S. Gund, D.P. Dubal, N.R. Chodankar, J.Y. Cho, P. Gomez-Romero, C. Park, C.D. Lokhande, Low-cost flexible supercapacitors with high-energy density based on nanostructured MnO_2 and Fe_2O_3 thin films directly fabricated onto stainless steel. Sci Rep (2015). https://doi.org/10.1038/srep12454
73. A. Tufan, T.A. Hansu, M. Akdemir, Production of a novel supercapacitor electrode material from Rheum ribes and its application. Bull. Mater. Sci. **45**, 1–9 (2022). https://doi.org/10.1007/s12034-022-02731-3